International Journal of Scientific & Engineering Research, Volume 7, Issue 12, December -2016
ISSN 2229-5518

Land Use Changes in the Eastern Nile Delta Region; Egypt Using Multi-temporal Remote Sensing Techniques

Mohsen M. Ezzeldin, Kassem S. El-Alfy, Hossam A. Abdel-Gawad, Mahmoud E. Abd-Elmaboud

Abstract-- Sustainable development in any region depends on authoritative monitoring of land cover change information. In this study, a hybrid classification methodology and post-classification change detection techniques were applied to five temporal data sets of images Landsat images acquired in 1984, 1990, 1998, 2006 and 2015, respectively, to map and monitor land cover changes in patterns related to agricultural development, water resources management and urban expansion in the desert fringes of the Eastern Nile Delta region of Egypt. Each temporal data set consists of two Landsat scenes, which were mosaicked to cover the whole region. Four different supervised classification algorithms were implemented to produce five land use maps. The maximum likelihood method showed higher classification accuracies in comparison with other methods. Post-classification comparison of these maps was used to obtain 'from–to' change detection maps. The results show that the rapid increase changes occurred among two land cover classes (urban, and agricultural land) led to shortages in the desert land area because land reclamation and the construction of new cities in the desert. Increase in urbanization led to the agricultural land degradation due to urban encroachment at the fringes of urban centers. Slight land cover changes were detected between marshland and surface water land cover classes.

Keywords-- Remote sensing; Image classification; Change detection; Land use; El-Manzala Lake; Eastern Nile Delta.

1 Introduction

Population growth on a global scale is imposing more stress on environmental resources, such as water resources. Over the century, the total population of Egypt increased from 11 million in 1907 to 90 million in 2015, according to the Central Agency for Public Mobilization and Statistics [1], making it the most heavily populated country in the Arab World and the third biggest in Africa. A recent report published by the World Bank, 2014 places population growth rates at close to 2.1% per year. The major part of this increase was concentrated in the Nile Delta region. The Nile Delta is the delta formed in Northern Egypt (Lower Egypt) where the Nile River spreads out and drains into the Mediterranean Sea. The Nile Delta is one of the oldest intensely cultivated areas on earth. It is very heavily populated, with population densities up to 1600 inhabitants per square kilometer [2], which exert profound pressure on natural resources of land and water. This overpopulation cause serious socioeconomic problems such as high unemployment, undermining rising living standards and crime rate [3].

The Egyptian government has started plans to regulate this situation since 1980s by redistributing the population by applying an efficient horizontal urban expansion along the desert areas and near the border of the Nile delta. The target of this policy is reducing the pressure on the old and highly productive agricultural land, reducing population density in the populated areas and decrease pollution sources by construction industrial areas outside the Nile valley and delta. Consequently, determining the direction and the rate of land cover conversion is necessary for the development planner in order to establish rational land use policy. For this purpose, the temporal dynamics of remote sensing data can play an important role in monitoring and analyzing land cover changes [3]. Remote sensing data provide an improved source for derivations of land use due to their reproducibility, internal consistency and coverage in locations where ground based knowledge is sparse [4], [5].

For many years, land-cover mapping has produced records of maps and atlases that have been used to monitor global models [6]. Remote-sensing technology and geographic information systems (GISs) have greatly facilitated investigation and monitoring of land-use/land-cover changes from satellite data requires effective and automated change detection techniques [7]. Various factors such as image quality, data analysis methodology, reading techniques and numerous temporal and phonological considerations significantly influence the character of the resulting geospatial information [8]. Although the accuracy of the resulting change maps is subject to error propagation and is dependent on the accuracy of the input classification maps, the individual classified images constitute a historical series that can be used in applications other than change detection [9],[10]. Digital change detection is the process of determining

- *Mohsen M. Ezzeldin is Prof. of Hydraulics, Irrigation & Hydraulics Dept., Faculty of Engineering, Mansoura University, Egypt. E-mail: mohsen-ezzeldin@hotmail.com*
- *Kassem S. El-Alfy is Prof. of Hydraulics, Irrigation & Hydraulics Dept., Faculty of Engineering, Mansoura University, Egypt. E-mail: amrorana2003@yahoo.com*
- *Hossam A. Abdel-Gawad is Associate prof., Irrigation & Hydraulics Dept., Faculty of Engineering, Mansoura University, Egypt. E-mail: hossamgawad@yahoo.com*
- *Mahmoud E. Abd-Elmaboud is Assistant Lecturer, Irrigation & Hydraulics Dept., Faculty of Engineering, Mansoura University, Egypt. E-mail: Mahmoud_elsayed717@yahoo.com*

and/or describing changes in land cover and land-use properties based on co-registered multi-temporal remote sensing data. The basic premise in using remote sensing data for change detection is that the process can identify changes between two or more dates that is uncharacteristic of normal variation. Numerous researchers have addressed the problem of accurately monitoring land-cover and land-use change in a wide variety of environments [11], [12], [13].

Many studies have discussed the significance of multi-temporal Landsat Thematic Mapper (TM) /Enhanced Thematic Mapper Plus (ETM+) data on land cover and land use changes in arid, semi-arid and agricultural productive land [14], [15] and [10]. [16] used Ten years of daily, continental scale satellite remote sensing data to assess and analyze land cover changes in the African continent between 1982 and 1991. The study showed that continuous unidirectional change process affected less than percent of Sub-Saharan regions during the study [17]) Used Landsat TM data to explore the impacts of land management policies on vegetation structure in two study areas in the southern Kalahari desert in South Africa in the period from 1989 to 1994. [18] studied land cover changes in the lake regions of central/south Ethiopia uses aerial photographs dated 1972 and 1994 Landsat TM image and multidisciplinary field survey. [19] combined black and white aerial photographs with fieldwork and GIS to monitor land cover changes covering 56 years (1940–1996) in parts of Bogota, Colombia. [20] used remote sensing techniques over a period of 26 years, from 1987 to 2013 to track land-use and land cover changes of the Ahwaz County in southwestern Iran. For this, ISODATA algorithm and Maximum Likelihood were initially used for unsupervised and supervised classifications of the satellite images. [21] assessed the spatio-temporal dynamics of land cover/land used changes in the lower Mekong Delta over the last 40 years with the coastal Tran Van Thoi District of Ca Mau Province, Vietnam. [22] evaluated land use/cover changes in Islamabad, Pakistan from 1992 to 2012 using two satellite images, and classifying them via supervised classification algorithm and finally applying post-classification change detection technique in GIS. The results observed increase in agricultural areas, built-up area and water body from 1992 to 2012.

Also, from studies in Egypt, [23] used satellite imagery to highlight agricultural boundaries and monitor the reclamation process. [24] used field calibrated, multi-temporal NDVI features derived from ten Landsat TM images dating from 1984 to 1993 to assess land cover changes in Egypt. The study showed a high rate of reclamation in the period 1986–1993 and a low rate of conversion of agricultural productive land to new urban areas between 1984 and 1990. [3] mapped land cover changes in the Northwestern coast of Egypt by applying maximum likelihood supervised classification and post-classification change detection techniques to Landsat images acquired in 1987 and 2001, respectively. [10] mapped and monitored land cover change patterns related to agricultural development and urban expansion in the desert fringes of the Eastern Nile Delta region by applying the methodology of post-classification change detection on three Landsat images of different time periods (1984, 1990 and 2003). The results show that agricultural development increased by 14% through the study period and the increase in urbanization (by 21 300 ha) during 1990–2003. [25] have used several Landsat images of different time periods and processed these images in ERDAS and ARC-GIS software to analyze the changes in the shores of the Lake Nasser, Egypt. [26] used land satellite images to study the urban sprawl and its impact on agricultural land in Qalubiya Governorate. They performed Post classification change detection technique to produce change image through cross-tabulation. [27] accreted characterize land-use changes in the Desert Fringes of Western Nile Delta region over number of years using object-based image classification approach. They applied Unsupervised followed by supervised classification separately to the acquired satellite images. The results showed that using satellite images to produce land-use maps is relatively cheap, accurate and fast. Also, change detection map can provide a powerful tool for planning, monitoring groundwater development and help to design a suitable exploration plan.

The objectives of this work are to mapping most important land cover as six classes (desert, Agriculture, Fallow, urban, Water and Marshland); observation changes in land use in the study area during following periods: of 1984-1990, 1990-1998, 1998-2006 and 2006-2015 using a post-classification change detection approach; used the results of the change detection to investigate the dominant trends in land-use development in the East Nile Delta and to identify zones that exhibit land cover change and determine the causes of the changes through spatial comparison of the land-use maps produced.

2 Materials and methods

2.1. Study area

The area of study occurs at the northeastern part of the Nile Delta and is bounded to the east by the Suez Canal, to the north by the Mediterranean Sea and El-Manzala Lake, to the west of the Damietta Branch of Nile River and to the south by the Cairo-Suez Desert Road. It is located between latitudes 30˚00'and 31˚30'N and longitudes 31˚00'and 32˚30'E and covers an area of about 15,000 km2 (Figure 1A,B). The topography of the

International Journal of Scientific & Engineering Research, Volume 7, Issue 12, December -2016
ISSN 2229-5518

northeastern Nile Delta is characterized by a low relief, and its surface slopes gently towards the northerly direction, while it holds a rolling shape towards the south, where the ground climbs up to a moderately elevated plateau with elevations that range between 2 m and 24 m above sea level (Figure 1B). The climate is hot, dry and rainless in summer and mild with some showers in winter. It is considered as arid to semi-arid. The mean monthly temperature ranges from about 120C in winter to 270C in summer. Mean yearly rainfall ranges between 20 and 100 mm [28], [29]. The main surface features in the survey area are active and fallow agricultural areas, urban shopping malls, sandy desert, fresh water canals, saltwater bodies, and marshland [10].

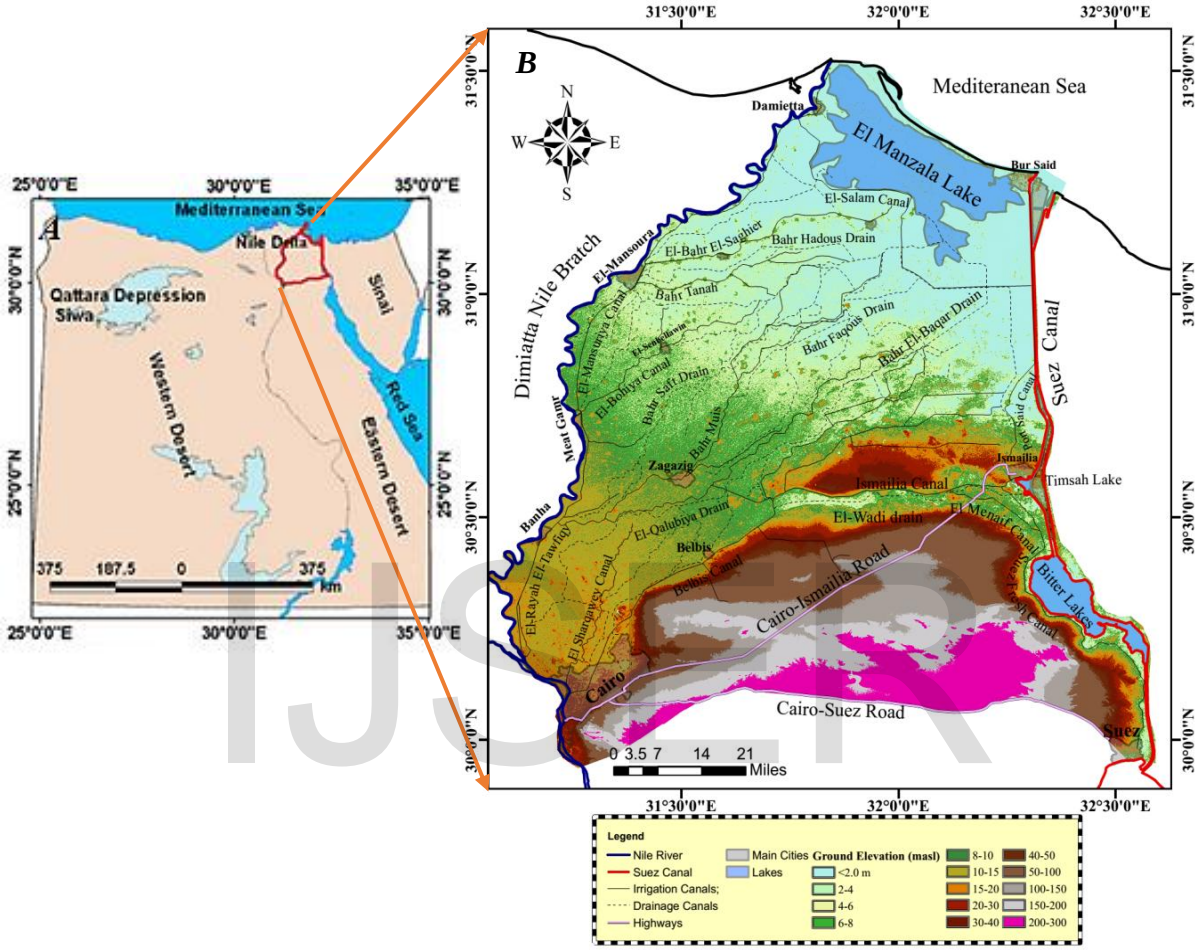

Fig. (1): (A) Map of Egypt, and (B) Location map and digital elevation model of the Eastern Nile Delta region, Egypt.

2.2. Data sets

The image data was acquired at unequal intervals between1984 and 2015, covering a time span of 31 years and was downloaded from the United State Geological Survey (USGS) Global Visualization Viewer website. The images have been acquired in summer season and in good quality, with no effective clouds [30]. During this time, most agricultural fields are active and green, which maximizes the spectral difference between the fields and bare soil or urban areas. Five satellite images consist of two scenes, first fall within path 176 and row 39 and other fall within path 176 and row 38 of the Worldwide Reference System (WRS), were acquired as shown in Table1 and Figure (2): three from the Landsat_4/TM (30 m spatial resolution) acquired in 1984, 1990 and 1998; one Landsat_7/ ETM+ (30 m spatial resolution) acquired in 2006; one Landsat_8/OLI (30 m spatial resolution) acquired in 2015. All image scenes were subjected to image processing using ENVI software version (5.3).

2.3 Image processing

Firstly, all images were checked against any defects such as striping. The image of 2006 already had gaps in all bands. Then, gaps were filled as shown in Figure (3). All images were clipped to include our study area. After that, all images were corrected geometrically and radiometrically.

International Journal of Scientific & Engineering Research, Volume 7, Issue 12, December -2016
ISSN 2229-5518

Table 1. Details of the satellite images used in this study.

Acquired data	Spacecraft/Sensor	Path/Row	Pixel Size (m)	Coordinate System/Datum	Zone
1984-09-20	LANDSAT_4/TM	176/ 39	30	UTM/WGS 84	36
1984-09-20		176/ 38			
1990-08-04	LANDSAT_4/TM	176/ 39	30	UTM/WGS 84	36
1990-08-04		176/ 38			
1998-09-11	LANDSAT_4/TM	176/ 39	30	UTM/WGS 84	36
1998-09-11		176/ 38			
2006-08-24	LANDSAT_7/ETM+	176/ 39	30	UTM/WGS 84	36
2006-08-11		176/ 38			
2015-08-09	LANDSAT_8/OLI	176/ 39	30	UTM/WGS 84	36
2015-07-24		176/ 38			

2.3.1 Geometric Correction

Change detection analysis is performed on a pixel-by-pixel basis; therefore accurate per-pixel registration of multi-temporal satellite data is essential because registration errors could be inferred as land use changes, leading to an overestimation of actual change [31] and, [26]. The Landsat images used in this study are ortho-rectified products. They are indeed in the World Geodetic System (WGS_84) datum and the Universal Transverse Mercator (UTM) projection system. The assessment of the geometric quality of the images by superimposing linear objects such as (road intersections, prominent geomorphologic features and river channels) permitted to observe significant discrepancies in the images. So, it was better to geo-reference all images sets using digital topographic maps (1:50,000) covering the Nile Delta, produced by the Egyptian General Survey Authority (EGSA) [32], [26] and [30].

Using the Environment for Visualization Images (ENVI) 5.3 image processing software package, the topographic map in a digital format produced in 1993 was firstly geo-referenced and rectified to a common UTM coordinate system. It was used as a base map to geo-reference the Landsat image acquired in 1990 through image to map referencing. Then, the Landsat TM image in 1990 was considered as the master image that was utilized to register the other images through image-to-image registration. A total of at least 60 ground control points (GCP) from digital topographic maps was examined and matched with all images. Figure 4 shows the distribution of the ground control points on the Landsat image in 2015. These points included: road intersections, river channels and prominent geomorphologic features. After rectification, the root mean square error (RMSE) was found not to exceed the 0.5 pixel threshold defined by [33], revealing a high geometric matching of the images. The RMSE could be defined as the deviations between GCP and GP location as predicted by the fitted-polynomial and their actual locations [3].

2.3.2 Radiometric Correction

To achieve an accurate radiometric correction, first, the atmospheric scattering correction was performed on the images using the dark-object subtraction method to correct any atmospheric interference caused by haze, dust or smoke [34]. Then, the current radiometric correction was implemented in one step using radiometric correction tool in ENVI software, which combines the sun and view angle effects, and the sensor calibration with the atmospheric correction. The needed parameters (offset/gain, sun elevation, and satellite viewing angles) are included with the Landsat metadata documentation.

2.3.3 Mosaic and mask

After radiometric correction, the two scenes of each data set were mosaicked using linear contrast stretching and histogram equalization to create a single image covering the whole study area from each data set [35]. Finally, the five images were spatially resampled with nearest-neighbor resampling to a 4929×5847 pixel rectangle that completely enclosed the study area. Within this rectangle, areas adjacent to and surrounding the study area were masked out so that they would not be included in the classification and change detection processing.

2.4 Image Classification

Our classification scheme comprises six land-use classes representing the dominant land cover types in the study area (table 2). The selection of land-use classes are based on the land cover classification system for remote sensing data adopted by [10]. Before classifying, the spectral characteristics of each land cover class in the five input images were explored by computing average spectra for each class (figure 5).

International Journal of Scientific & Engineering Research, Volume 7, Issue 12, December -2016
ISSN 2229-5518

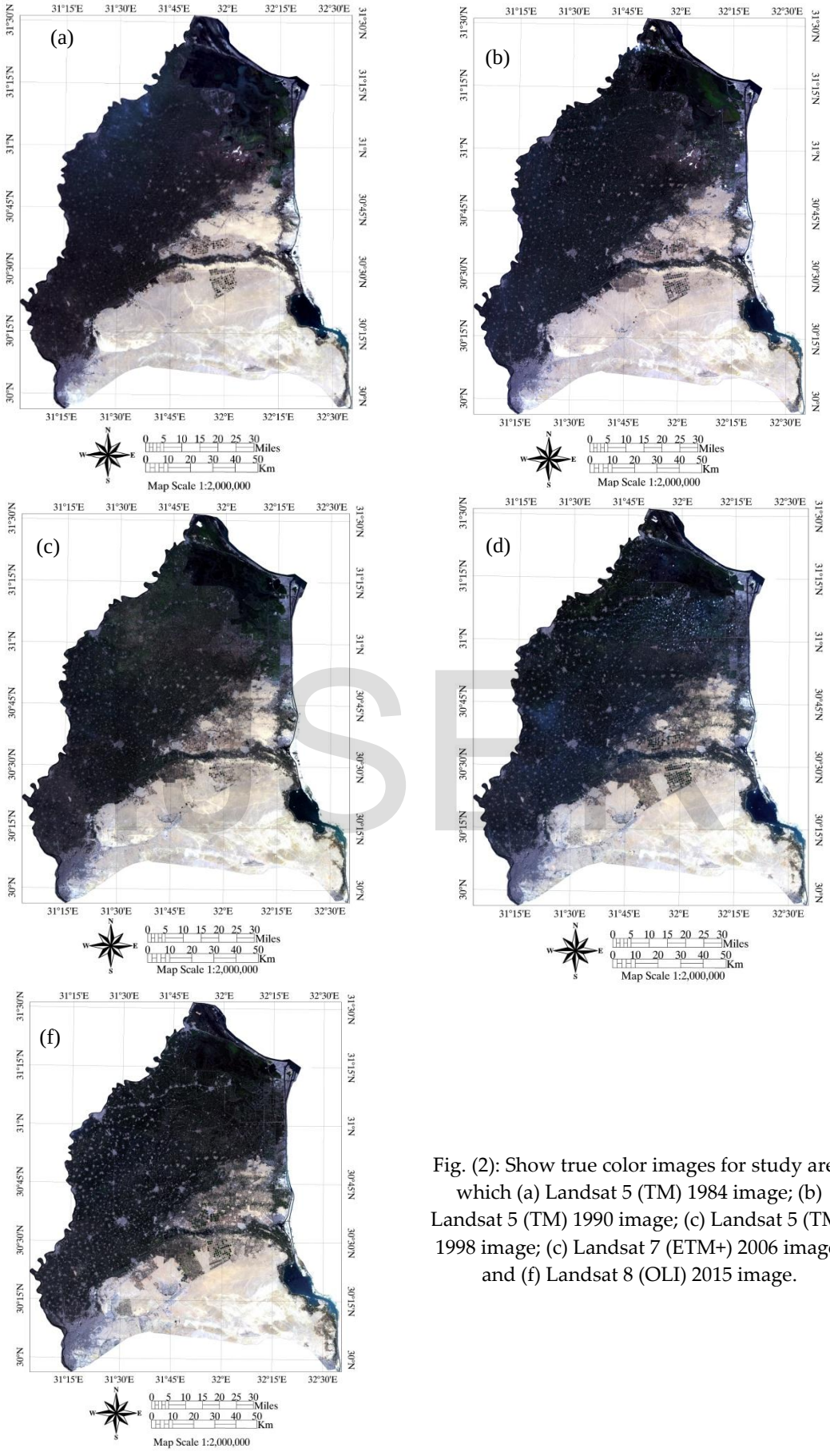

Fig. (2): Show true color images for study area which (a) Landsat 5 (TM) 1984 image; (b) Landsat 5 (TM) 1990 image; (c) Landsat 5 (TM) 1998 image; (c) Landsat 7 (ETM+) 2006 image; and (f) Landsat 8 (OLI) 2015 image.

International Journal of Scientific & Engineering Research, Volume 7, Issue 12, December -2016
ISSN 2229-5518

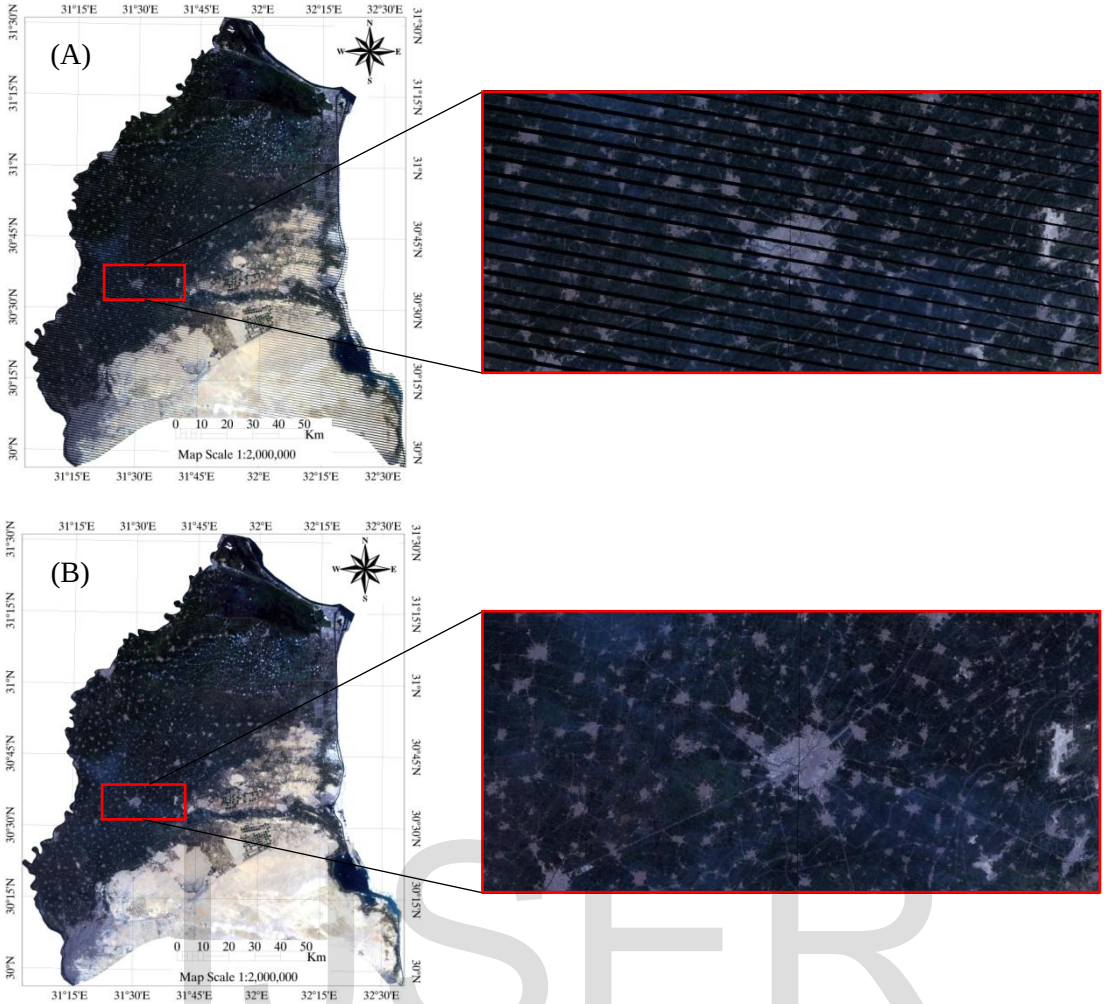

Fig. (3): (A) Landsat image (2006) before striping removal; and (B) after striping removal.

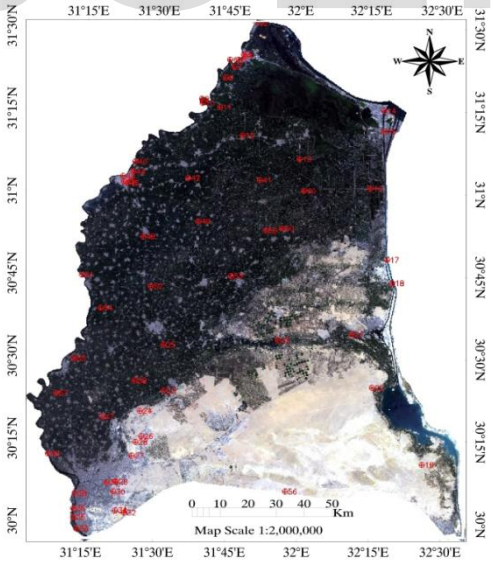

Fig. (4): Distribution of ground control points in the image (2015).

International Journal of Scientific & Engineering Research, Volume 7, Issue 12, December -2016
ISSN 2229-5518

Spectral analysis shows that the desert, agriculture and water classes are radiometrically distinct from each other and from the other classes. However, the fallow agriculture, marshland and urban classes are very similar to one another (figure 5). This spectral similarity can be explained by their substantial clay contents. Classification algorithms, therefore, may tend to misclassify fallow agricultural fields with urban or marshland. [24] described a similar problem arising from the similarity of low productivity lands and urban lands in the Western Nile Delta region.

Table 2. The land cover classification scheme used in this study (After [10])

Class	Description
Urban	Adobe and concrete structures (residential, commercial, Transportation, and other uses)
Agriculture	Crop fields and lawns
Fallow	Harvested and bare fields
Desert	Desert
Water	Lakes, canals, fish farms, and estuaries
Marshland	Wetland

To complete the change detection analysis, post classification change detection analysis was applied, which included image classification, change detection and accuracy assessment. Figure 6 presents chart for the procedures applied in this study as a typical post-classification change detection analysis.

In this study Hybrid supervised/unsupervised classification called"guided clustering" is used for land cover classification [36], [10]. In this tactic, the unsupervised interactive self-organizing data analysis (ISODATA) calculates class means evenly distributed in the data space, and then iteratively clusters the remaining pixels using minimum distance techniques. Means and reclassifies pixels with respect to the new means is recalculated in each iteration. This process continues until reaches to the maximum number of iterations [37].

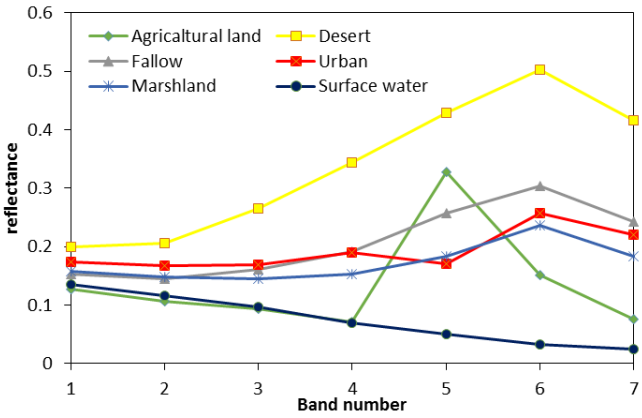

Fig. (5): Spectral plot for the five spectrally land cover classes.

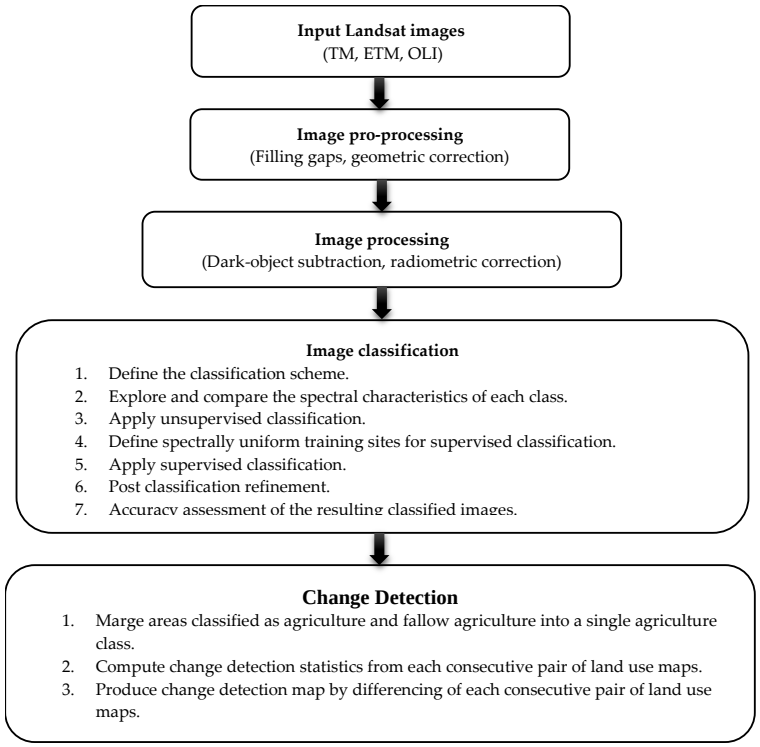

Fig. (6): Flow chart show steps applied in post-classification change detection analysis.

International Journal of Scientific & Engineering Research, Volume 7, Issue 12, December -2016
ISSN 2229-5518

The ISODATA gathering method enables reconnoitering of the spectral contents of an input image and automatically selects spectral groups [38]. Then a subscription file for the image is created using this information, which contains average spectra for each class determined by the unsupervised classification. These spectra were used to determine spectrally uniform training sites for a subsequent supervised classification algorithm [10]. Fortieth classes were obtained from the ISODATA analysis, some of which compatible with more than one of the land cover types in our classification scheme (Table 2). Post-classification signature assessment was therefore necessary to combine and separate the ISODATA classes into the new set of spectrally uniform training classes.

Supervised classification methods required much training data, so it is a difficult process [39]. Moreover, one of the most important factors in classifying the pixels is selecting training samples. As proven earlier the training samples are chosen from the ISODATA classes. Training samples were prepared for six classes as shown in (Table 2). The samples were exported to Google Earth to check the ground truth data of these training samples. Training samples were divided into two classes that one of them was used for classification and another for supervising classification accuracy (Table 3).

Table 3. The characteristics of training samples

Class name	Training simples area (m2)	Training simples area (Pixel)	Evaluation simples area (m2)	Evaluation simples area (Pixel)
Urban	558000	620	55800	62
Agriculture	778500	865	72000	80
Fallow	418500	465	51300	57
Desert	661500	735	64800	72
Water	571500	635	61200	68
Marshland	327600	364	45000	50

Supervised classification using four different classification algorithms, Maximum likelihood, Minimum distance, Mahalanobis Distance and Spectral Angle Mapper, was performed. Post-classification refinement of the resulting classified images was applied to the inaccurately classified pixels to increase the overall accuracy of the resulting land cover maps.

2.4.1 Maximum Likelihood

The maximum likelihood method is one of the most popular supervised classification methods used with remote sensing information [40]. This method supposes that the statistics for each class in each band are normally distributed and calculates the probability that a given pixel belongs to a specific class. Unless you select a probability threshold, all pixels are separated. Each pixel is assigned to the class that has the highest probability (that is, the maximum likelihood). If the highest probability is smaller than a threshold you specify, the pixel remains unclassified [41] and [37].

ENVI implements maximum likelihood classification by calculating the following discriminant functions for each pixel in the image [40]:

$$g_i(x) = \ln p(\omega_i) - \frac{1}{2}\ln|\sum_i| - \frac{1}{2}(x - m_i)^T \sum_i^{-1}(x - m_i) \quad (1)$$

Which: $g_i(x)$ = discriminant functions; i = classes; x = measurement vector of the candidate pixel; p (ωi) = probability that class ωi occurs in the image and is assumed the same for all classes; |Σi| = determinant of the covariance matrix of the data in class ωi; Σi-1= its inverse matrix; mi = mean vector and T = transposition function (matrix algebra).

2.4.2 Minimum Distance

The minimum distance technique uses the mean vectors of each end member and calculates the Euclidean distance from each unknown pixel to the mean vector for each class. All pixels are classified to the nearest class unless a standard deviation or distance threshold is specified, in which case some pixels may be unclassified if they do not meet the selected criteria [40].

The equation for classifying by Minimum distance is based on the equation for Euclidean distance:

$$d(x, m_i) = [(x - m_i)(x - m_i)]^{\frac{1}{2}}, \quad i = 1, \ldots M \quad (2)$$

Which: $d(x, m_i)$ = Minimum Distance; i = class; x = is measurement vector of the pixel to be classified; m_i = mean vector; and i = classes

2.4.3 Mahalanobis Distance

The Mahalanobis distance classification is a direction-sensitive distance classifier that uses statistics for each class. It is similar to the maximum likelihood classification, but assumes all class covariance is equal and therefore is a faster method. All pixels are classified into the closest ROI class unless you specify a distance threshold, in which case some pixels may be unclassified if they do not meet the threshold [40].

International Journal of Scientific & Engineering Research, Volume 7, Issue 12, December -2016
ISSN 2229-5518

The equation for the Mahalanobis Distance classifier is as follows:

$$d(x, m_i) = [(x - m_i)^t \sum^{-1} (x - m_i)]^{1/2} \quad (3)$$

Which: $d(x, m_i)$ = Mahalanobis Distance; I = class; x = is the position of pixel to be classified; m_i = mean vector; i = classes; T = transposition function (matrix algebra) and $\sum^{-1}$= inverse of the covariance matrix.

2.4.4 Spectral Angle Mapper

The Spectral Angle Mapper algorithm determines the spectral similarity between two spectra by calculating the angle between the spectra and treating them as vectors in a space with dimensionality equal to the number of bands. Spectral Angle Mapper compares the angle between the end member spectrum vector and each pixel vector in n-dimensional space. Small angles between the two spectrums indicate high similarity and high angles indicate low similarity [42]; [43]. The Spectral Angle Mapper method takes the arc cosine of the dot product between the test spectrums "t" to a reference spectrum "r" with the following equation [42]; [43]:

$$\alpha = \cos^{-1}\left(\frac{\sum_{i=1}^{nb} t_i r_i}{\left(\sum_{i=1}^{nb} t_i^2\right)^{1/2} \left(\sum_{i=1}^{nb} r_i^2\right)^{1/2}}\right) \quad (4)$$

Which: nb = the number of bands; t_i = test spectrum and r_i = reference spectrum.

2.5 Change Detection

Change detection can be defined as the process of identifying differences in the state of an object or phenomenon by observing it at different times [13]. In general, change detection involves the application of multi-temporal data sets to quantitatively analyze the temporal effect [44].

There are various ways of approaching the use of satellite imagery for determining change in urban environments [45]. The methods for change detection can be divided into pre-classification and post-classification techniques [13], [33], [46], [9], [47]. The pre-classification techniques apply various algorithms directly to multiple dates of satellite imagery to generate ‘‘change" versus ‘‘no-change" maps. These techniques locate where changes took place, but do not provide information on the nature of the change ([13], [9]. In other hand, Post-classification comparison methods use separate classifications of images acquired at different times to produce difference maps. ‘‘From–to" change information can be generated telling us how much change occurred or what areas changed from–to [48], [49], [38], [47]. In this work, Post-classification change detection is employed after classifying the five images separately.

Since our purpose is not to monitor the changes from agriculture to fallow agriculture, or vice versa, we merged areas classified as agricultural and fallow agriculture into a single agriculture class before proceeding with the change detection analysis.

Four change maps were compiled to display the specific nature of the changes between the classified images (1984–1990, 1990–1998, 1998-2006 and 2006-2015). The change detection classification maps were then cleaned up. This step is necessary for the refinement of the classification results, due to geo-registration errors that occur between different dates [35]. Post-classification refinement improved the overall accuracy of our classification maps based on two processes:

(a) Smoothing analysis, to removes salt and pepper noise effect throughout applying smoothing Kernel’s of 3×3 pixels. The square kernel’s center pixel is replaced with the majority class value of the kernel and;

(b) Aggregation analysis, to remove small regions throughout applying aggregation window of 9 pixels. Regions with a size of this value or smaller are aggregated to a larger adjacent pixels.

2.6 Accuracy assessment

Accuracy assessment for classification is carried out using confusion matrices [50]. A confusion matrix presents the relationship between the reference data and the resulting land cover map. It supplies information about errors of oversight, or producer’s accuracy, and commission, or user’s accuracy. The number of samples of each land-use class used to prepare the confusion matrix is used to determine the confidence level and the expected accuracy obtained from the confusion matrix approach [10]. For classification study, [50] suggested 75 or 100 samples per land-use class if there are more than 12 classes or the study area is larger than 400 000 hectares. In this study, for each land-use map, after eliminating reference stations located close to class boundaries, 50–80 samples of 10–15 pixels each were picked randomly from the reference stations of each land-use class to construct the confusion matrix. The result of an accurate assessment typically provides the users with an overall accuracy of the map and the accuracy for each class in the map. The percentage of overall accuracy was calculated using the following equation:

$$\text{Overall accuracy} = \frac{\text{Total number of correct samples}}{\text{Total number of samples}} \times 100\ \% \quad (5)$$

Beside the overall accuracy, classification accuracy of individual classes was calculated in a similar manner. The two approaches are user's accuracy and producer's accuracy. The producer's accuracy is derived by dividing the number of corrected in one class divided by the total number of pixels as derived from reference data. The

International Journal of Scientific & Engineering Research, Volume 7, Issue 12, December -2016
ISSN 2229-5518

producer's accuracy measures how well a certain area has been classified. It includes the error of omission which refers to the proportion of observed features on the ground that is not classified in the map. User's accuracy is computed by dividing the number of correctly classified pixels in each category by the total number of pixels that were classified in that category. The user's accuracy measures the commission error and indicates the probability that a pixel classified into a given category actually represents that category on the ground. Producer's and user's accuracy are derived from the following equation:

$$\text{Producer'S accuracy} = 100\ \% - \text{error of omission}\%$$
$$\text{User'S accuracy} = 100\ \% - \text{error of commission}\% \quad (6)$$

After computing confusion matrix in each iteration Kappa (K) coefficient is calculated. Kappa (K) coefficient is a measure the agreement between classification and ground truth pixels. This measure of agreement is based on the difference between the actual agreements in the confusion matrix [51]. The value of Kappa lies between 0 and 1, where 0 represents agreement due to change only. 1 represent the complete agreement between the two data sets. Negative values can occur, but they are spurious. It is usually expressed as a percentage (%). Kappa statistic can be a more sophisticated measurement to classifier agreement and thus gives better interclass discrimination than overall accuracy. The estimation of the Kappa coefficient was carried out using the following equation:

$$K = \frac{N\sum_{i=1}^{n} m_{i,i} - \sum_{i=1}^{n}(G_i C_i)}{N^2 - \sum_{i=1}^{n}(G_i C_i)} \quad (7)$$

Where :

- **i**: is the class number;
- **N**: is the total number of the classified pixels that are being compared to ground truth;
- $\mathbf{m_{i,i}}$: is the number of pixels belonging to the ground truth class **i**, that have also been classified with a class **i** (i.e., Values found along the diagonal of the confusion matrix);
- $\mathbf{C_i}$: is the total number of the classified pixels belonging to class **I** and
- G_i: is the total number of ground truth pixels belonging to the class.

In this way, the accuracy of the land-use maps produced by classification was assessed at several stages in the post-classification processing before carrying out change detection. The overall accuracy of the final classifications, including the user and producer accuracies and Kappa coefficients obtained from the confusion matrices, are shown in table 4.

3 Results and discussions

Supervised classification using different classification algorithms was performed. The overall accuracy and Kappa coefficients of each classification algorithm obtained from the confusion matrices are shown in table 4.

Maximum likelihood showed better classification results than other classification algorithms. The result of all classification algorithms, both of overall accuracies, and Kappa coefficients were increased gradually from TM 1984 toward OLI 2015. This could be explained due to the fact that the date acquisition of the fifth data set (OLI 2015) is relatively closer to the date of the training and validation point collection [35].

Table 4. Overall accuracies and Kappa coefficients of each classification algorithm

Year of acquisition	Classification algorithm							
	Maximum likelihood		Minimum distance		Mahalanobis Distance		Spectral Angle Mapper	
	Overall Accuracy (%)	Kappa Coefficient (%)	Overall Accuracy (%)	Kappa Coefficient (%)	Overall Accuracy (%)	Kappa Coefficient (%)	Overall Accuracy (%)	Kappa Coefficient (%)
1984	97.14%	0.9577	92.06%	0.8825	83.95%	0.7747	92.81%	0.8929
1990	97.70%	0.965	94.17%	0.9119	90.37%	0.8587	93.76%	0.9051
1998	95.74%	0.9348	91.77%	0.8746	84.75%	0.7797	92.69%	0.8876
2006	96.64%	0.9483	90.62%	0.8563	89.70%	0.8373	93.22%	0.8953
2015	98.00%	0.9668	93.30%	0.8883	93.10%	0.8879	93.64%	0.8928

Figure (7) show the final products of the hybrid classification were five land cover maps in which the spatial distribution of the land covers classes for the years 1984, 1990, 1998, 2006 and 2015 using maximum likelihood as a supervised classification algorithm. The land use maps show that the agriculture and desert classes cover extensive areas. In the 1984 land cover map there are 543197 ha of desert available for reclamation and development.

International Journal of Scientific & Engineering Research, Volume 7, Issue 12, December -2016
ISSN 2229-5518

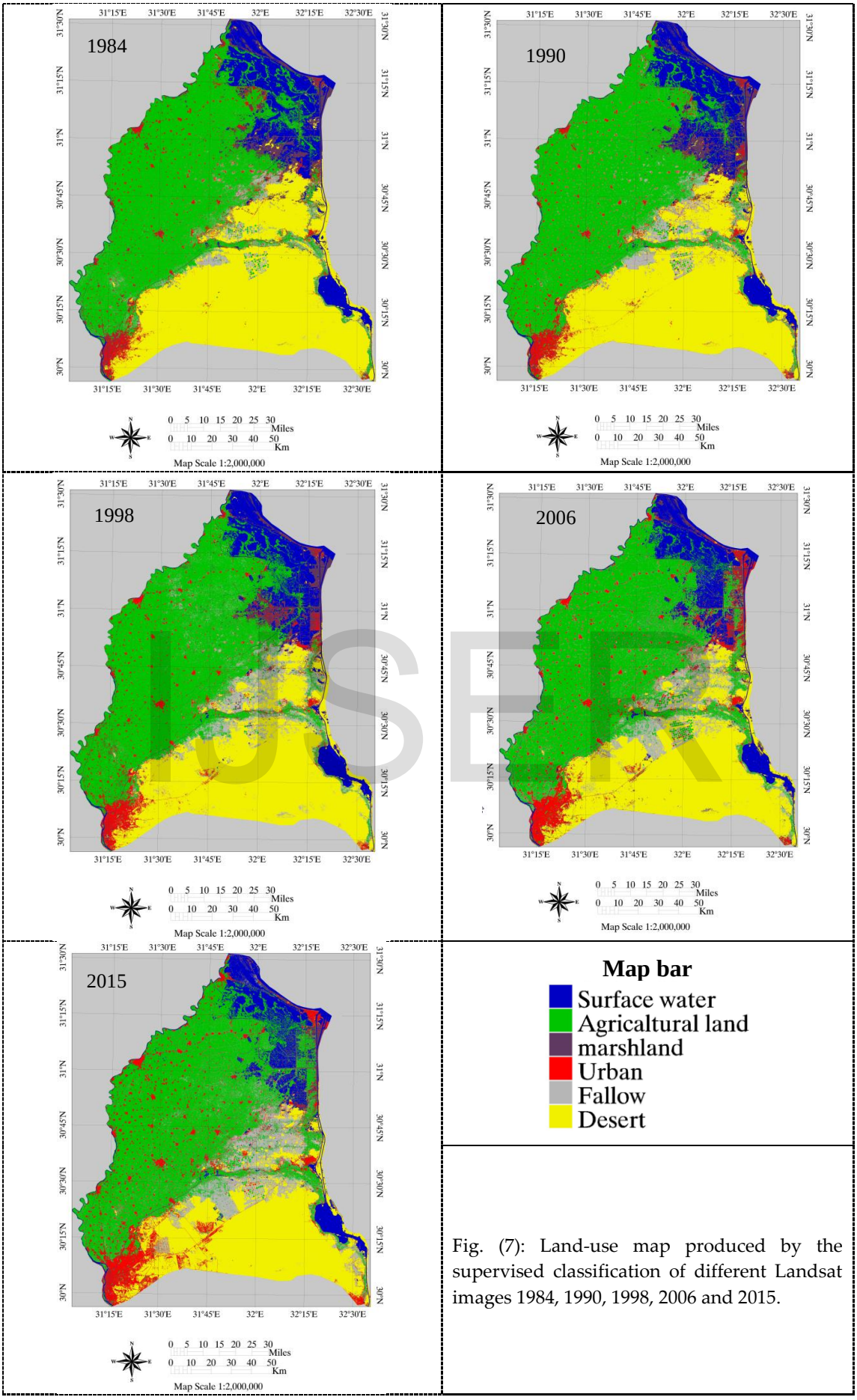

Fig. (7): Land-use map produced by the supervised classification of different Landsat images 1984, 1990, 1998, 2006 and 2015.

International Journal of Scientific & Engineering Research, Volume 7, Issue 12, December -2016
ISSN 2229-5518

Several thousand hectares of this land lie to the north and south of Ismaelia Canal. In the 2015 this area decreases to 381045 ha, as a result of the increase in land reclamation and construction of new residential cities in the area east of the Nile Delta such as the Tenth of Ramadan, Badr, Al Shrouk, Al Obour, New Heliopolis, new Cairo, and Al Salheyah cities. Most of these areas are developed using groundwater resources and areas lies between the Cairo–Ismaelia and Cairo–Suez desert roads are developed by using surface water resources (Figure 7).

On the other hand, in the northern part of the study area, the surface water and marshland classes are often found adjacent to one another. As shown in Figure (7), El-Manzala Lake is gradually diminished in its area from the year 1984 to 2015, as a result of the drying and road construction and agricultural and urban expansion. The drill-Salam Canal and the establishment of the international coastal road across the lake was one of the main causes of the shrinking area of the lake and divide operations as well as land reclamation for agricultural purposes.

For areas classified as urban lie mostly disseminated within areas classified as agricultural specially lands in the western part of the study area (Figure 7). The overvaluation of the urban area in classification maps of the year 2006 and the year 2015 is due to the fact that approximately 85 % of the irrigation network system (main and secondary canals) in the study area is constructed from concrete materials, which are the same materials, used for building construction. This is why the cleanup analysis is mandatory to improve the classification accuracy [35], [52].

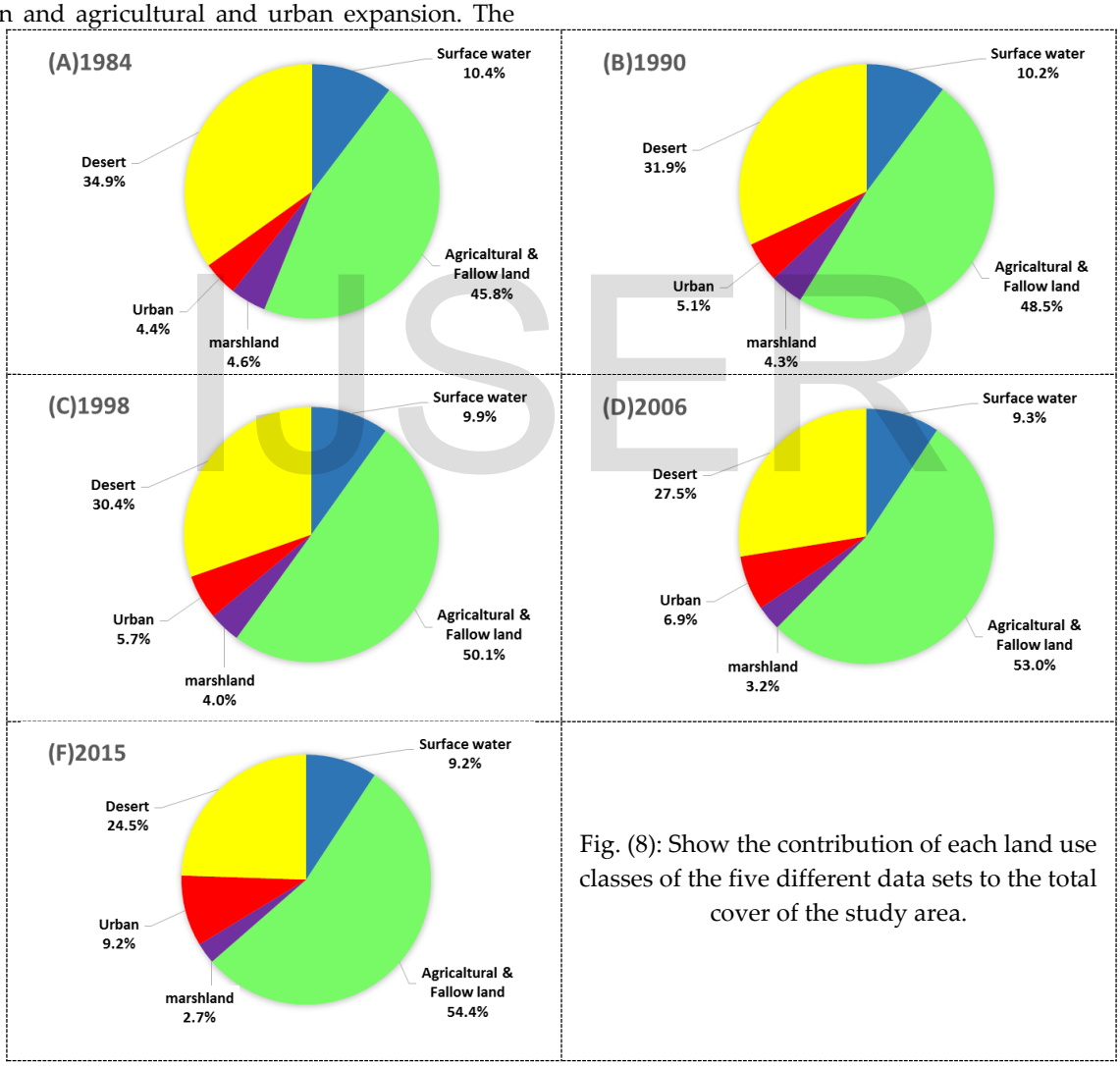

Fig. (8): Show the contribution of each land use classes of the five different data sets to the total cover of the study area.

Data set acquired in 1984 considered as reference point to the current changes in land use of the Nile Delta region due to the fact that the mega agricultural expansion projects started in the year 1985 as it is reported by the Ministry of Public Work and Water Resources, Agricultural Policy Reform Program ''MPWWR'' in 1998 [35].

In the year 1984, the summation of the agriculture land and fallow represent nearly 46% of total area. Between year1990 and 2006, the noticeable expansion of both agricultural land, fallow and urban area was

International Journal of Scientific & Engineering Research, Volume 7, Issue 12, December -2016
ISSN 2229-5518

directed against the total area of the desert land cover and with slight decrease in the total area of the surface water and marshland was noticed. The final changes in the year 2015 demonstrate further loss in the total area of the desert land cover against the increase in total area of urban. Steady state in the total area of the agricultural and fallow land accompanied with slight decrease in the total area of the surface water and marchland was noticed (Figure 8).

Post-classification comparison is demonstrated in Figures (9 and 10) explains the thematic changes occurred in different land use classes that exist in the study area. The changes in land use in term of percentages between the year 1990 and 1984 are demonstrated in Figure (9-a). A strong loss in desert total area was induced by the amplification of both agricultural land and urban area. According to Figure (10-a), the expansion of the agricultural land was toward the desert, while the expansion of urban areas was toward the agricultural land. The slight decrease in the total area of surface water took place toward the agricultural land also and marchland. Land use changes that occurred between the years 1998 and 1990 (Figure 9-b) and the years 2006 and 1998, detect additional loss in the total area of the desert in addition to decrease in surface water and marshland against an increase agricultural land total area and slight increase of urban areas (Figure 10-b,c). Final stage of change detection demonstrated in Figure (9-d), the total area of the urban was roughly increased by only 2.26 % over nearly one decade which is rather similar to the decrease of the desert area (2.86 %), the expansion of urban areas was noticed to be against the desert and marshland (Figure 10-d).

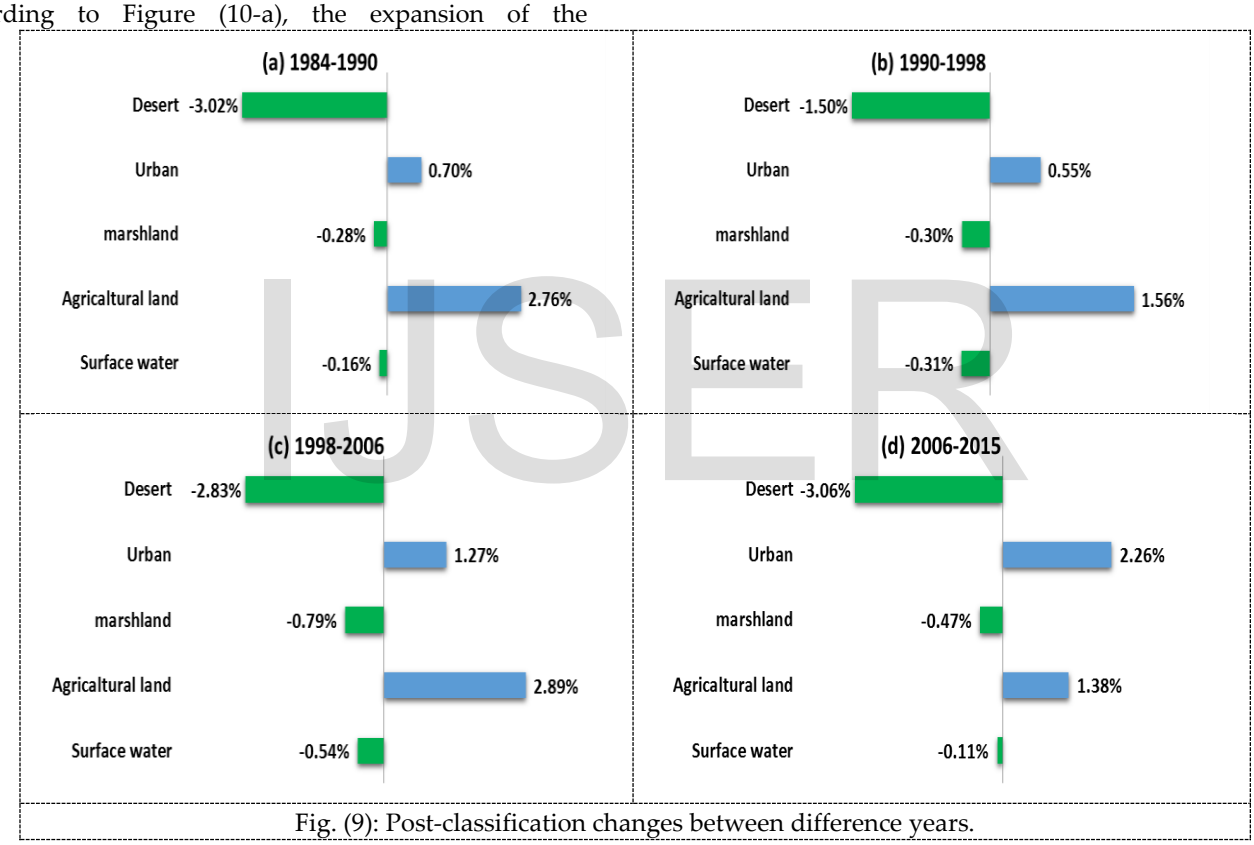

Fig. (9): Post-classification changes between difference years.

The results of change detection analysis (Figures 9 and 10) show a systematic increase in agricultural activities between 1984 and 2015, arising from national agricultural development plans. Increasing in agricultural land and fallow occurred during 1984–1990 by about 43000 ha, about 24328 ha during 1990–1998, about 45006 ha during 1998–2006 and minimum increase about 21450 ha during 2006–2015 at a respective average annual rate of 7167, 3041, 5625 and 2383 ha a-1. In recent years, an area of reclaimed land has increased, but this increase is offset by the lack of agricultural land in delta due to the increase in urban area.

The changes detected maps (Figure 10) are heavy and granulated in texture, referencing a large region containing a concentration of many areas of localized change, especially in area between El-Manzala Lake and Suez Canal. In the 1984–1990 change maps, the sites of change are more scattered, most likely due to the short time period between the two dates. During 1990–1998 and 1998-2006 the main expansion of agricultural land occurred at the expense of desert areas around the eastern part of Ismaelia Canal and the area between Ismaelia Canal and the Bahr El Baqar Drain, also converted the former marshland at the western border of Lake El Manzala to agriculture (Figures 10-b and c). During 2006–

International Journal of Scientific & Engineering Research, Volume 7, Issue 12, December -2016
ISSN 2229-5518

2015, this period is characterized by expansion of urban area by razing agricultural land and also expansion in the construction of new cities in desert around Cairo city.

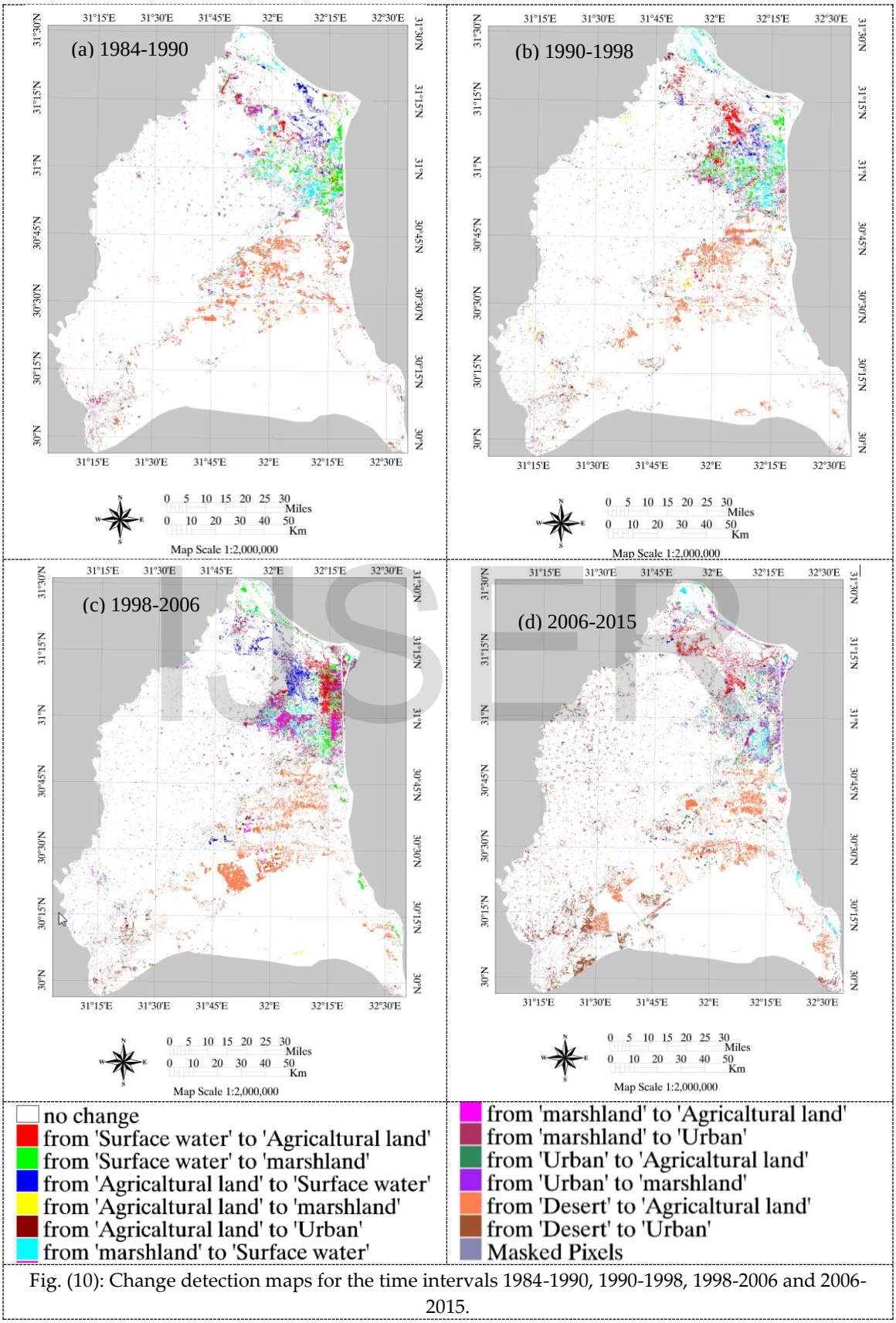

Fig. (10): Change detection maps for the time intervals 1984-1990, 1990-1998, 1998-2006 and 2006-2015.

International Journal of Scientific & Engineering Research, Volume 7, Issue 12, December -2016
ISSN 2229-5518

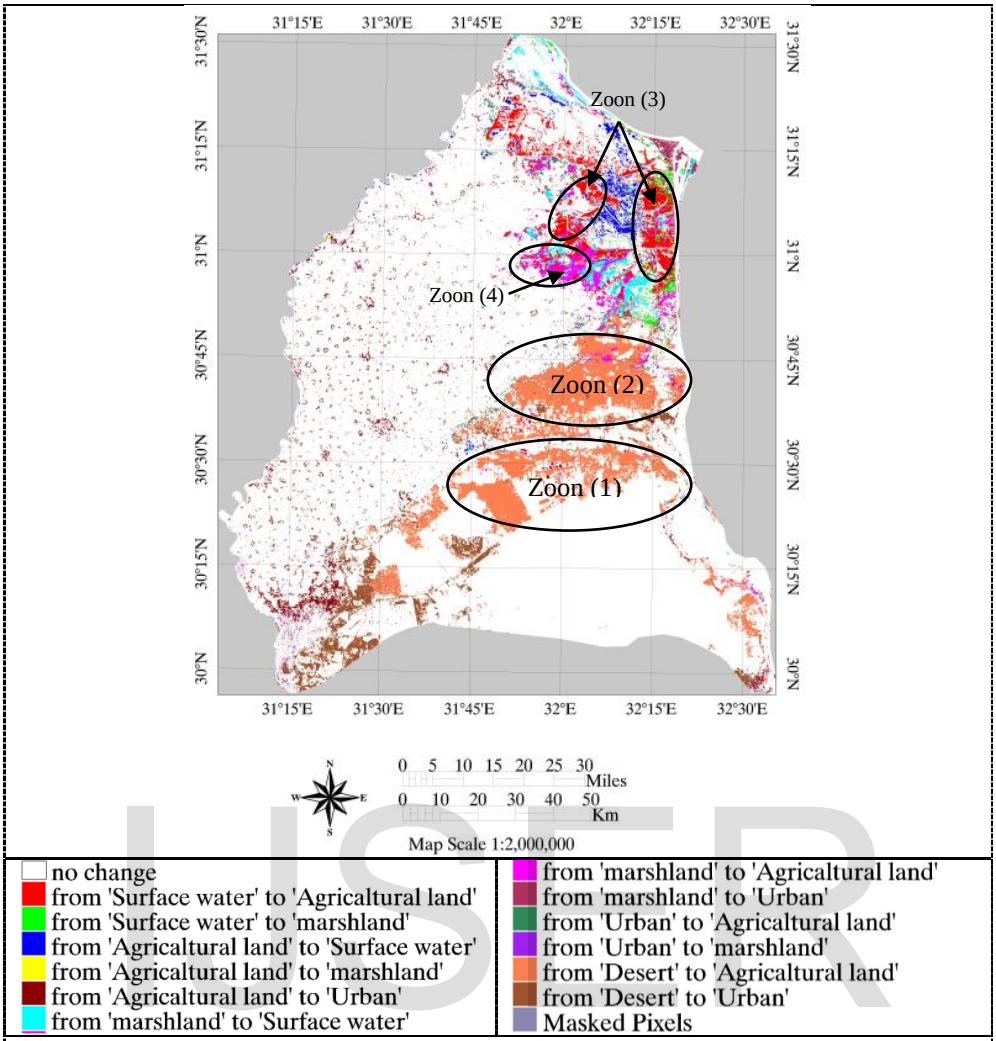

Fig. (11): Change detection maps for the time interval 1984-2015.

In general, a key factor in the economic development area east Nile Delta is to conciliate the increasing population density and the need for maintaining food security and creating new jobs. So, between the year 1984 and 2015 there are many areas of localized change as shown in the change detection map (Figure 11). As shown in this figure, there are four important areas of change appears extensive agricultural development. Zoon (1) covers more than 45320 ha to the south and the south-east of Ismaelia Canal. Zoon (2) enclosed by the courses of the Bahr El Baqar Drain from the west, the Ismaelia Canal from the south and the Suez canal from the east. It represents the most intense agricultural development in the East Nile Delta region and includes 74152 ha in the area. Zoon (3) occupies 39269 ha in the north and the north-east corner of the study area and was formerly a part of Lake El Manzala that has been converted to agricultural land. Finally, the wetland that has been developed for agricultural purposes using surface water irrigation is shown in Zoon (4) covers more than 22690 ha to the south of Lake El Manzala. The main crops in these areas are fruits, vegetables, atom, rice and wheat and their dependent agro-industrial activities, such as food industries (ESIA 2007).

In zoon (1) agricultural development depended on surface water from Ismaelia Canal, because the groundwater salinity in some areas is relatively high (> 4000 ppm; [10]. Between years 1984 and 2015, various seepage areas were appeared in the lowlands to the north of zoon (1) as shown in the comparison between 1984 and 2015 images, Figure (12). This is due to the soil is dominantly sandy in this region and this allows drain some of the water that used for irrigation, so the zoon (1) become working as recharge areas. Since zoon (1) is topographically high relative to areas to the north, the recharging water may affect the groundwater flow and distribution of salinity in the adjacent topographically low areas.

International Journal of Scientific & Engineering Research, Volume 7, Issue 12, December -2016
ISSN 2229-5518

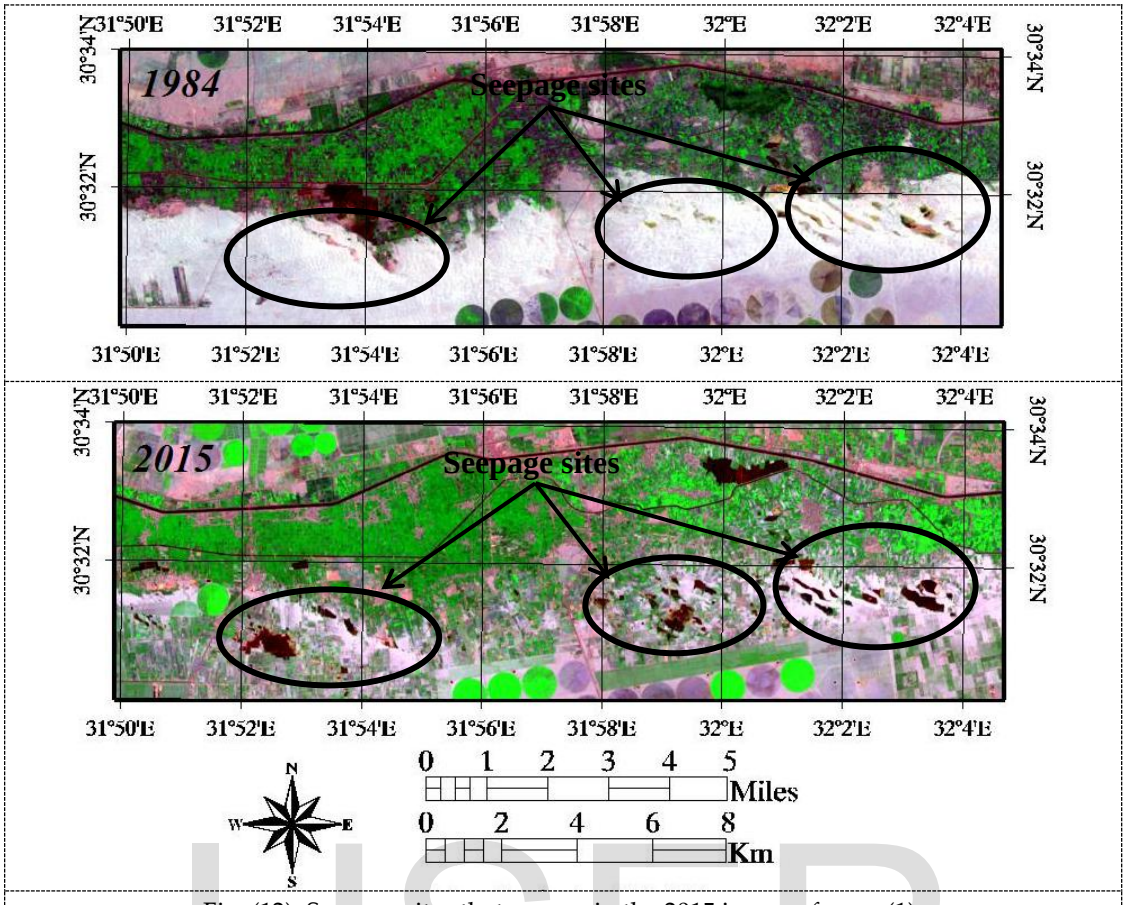

Fig. (12): Seepage sites that appear in the 2015 image of zoon (1).

On the other hand, the development of Agricultural lands at Zoon (2) depend on both surface and groundwater resources. The same environmental impacts related with the major land-use changes at zoon (1) is also appeared in zoon (2), where some seepage areas were appeared in the low lands of zoon (2) as shown in Figure (13). In general, the total areas of desert which change to seepage area during the 1984-2015 periods equal to 4294.0 ha. Figure (14) shows some field photos of seepage sites that appear in zoon (1) and zoon (2).

From economical side, comparing with the old lands in the inner Nile Delta region, reclaiming the desert in zoon (1) and (2) into agricultural lands required high costly irrigation networks supplying water from River Nile to new agricultural lands in this zones and also higher water consumption for agricultural use due to increased evapo-transpiration in the desert [53]; [35]. From quantitative side, the total water requirements for old land in the total Nile Delta region (4.5 million Fadden) is about 47.4×1012 m3 with irrigation efficiency of 80 % while the total water requirements for the new land in east and west of Nile delta (only about 0.6 million Fadden) is about 6.9×1012 m3 with an irrigation efficiency of 90 % which means that the new land requires about 14.5 % of the total water budget [35].

During the last two decades, the region surrounding Lake Manzala has seen social and economic variations effect on land use change as illustrated in the zoon 3 and 4. This changes has been driven by drying policy. Drying policy, which is considered one of the most influential and destructive policies of Fisheries, led to change the topography of the lake and its collapse has hurt so irreparable damage to the national economy to increase the large losses in productivity and to bridge the food gap, which cannot be bridged without the import from abroad. In addition to the social damage as a result of a large segment of the fishermen crashes to the lack of space and poor fish stocks consequent. Drying led to the exit Ismailia Governorate from El Manzala lake where they were drying Um El Resh area and exit other areas such as logic San El Hagar and Husseiniya and Bahar El Baqar, which was famous during the seventh and eighth decade of last century the most famous fish farms, which have been converted to agricultural land. As has been drying the eastern area of the lake El Manzala from south of Port Said, even Qantara, which was known project Nasser, a fish farm, which led to the exit area of 25,000 fed for agricultural use. Drying for the purpose of urbanization to meet the need of some governors to the amount of land a private Port Said for urbanization, which withheld thousands of feddans, and also for the

International Journal of Scientific & Engineering Research, Volume 7, Issue 12, December -2016
ISSN 2229-5518

purpose of construction of new roads, such as Damietta Port Said Road an alternative to the coastal road, leading to the lake divided into two parts. Moreover, the establishment of Al-Salam Canal south of the El Manzala Lake, which transfers the Nile river water to the Sinai Peninsula, has displayed lake to other deductions amounted to 50,000 fed south of Port Said in addition to the 62,000 fed North Husseinieh addition to the areas that have been isolated from the lake in Damietta.

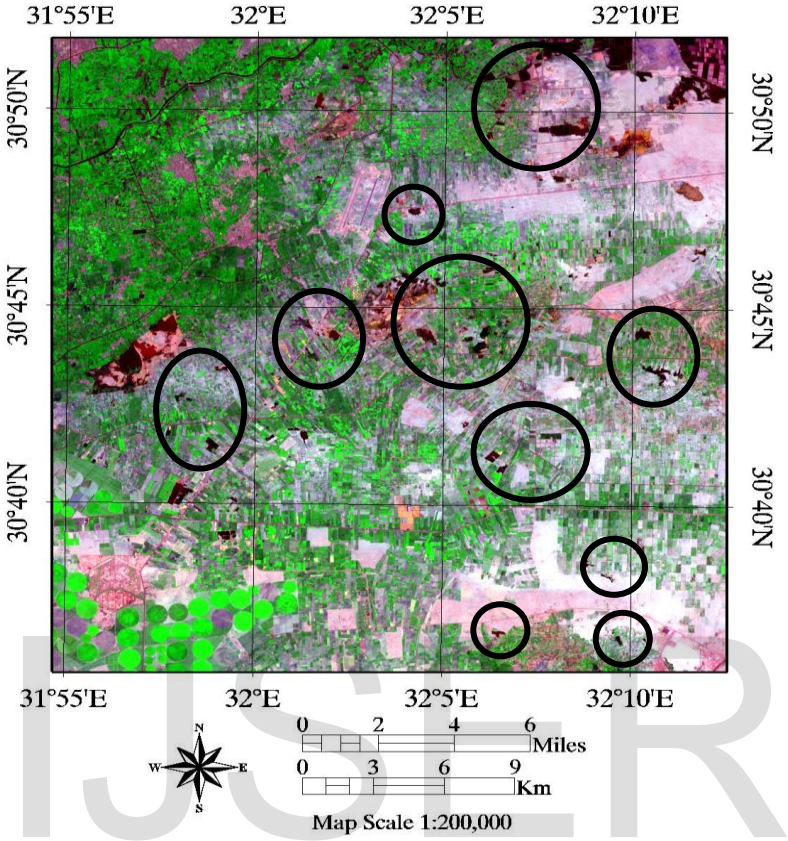

Fig. (13): Seepage sites that appear in the 2015 image of zoon (2).

Fig. (14): Some field photos of seepage sites that appear in zoon (1) and zoon (2).

International Journal of Scientific & Engineering Research, Volume 7, Issue 12, December -2016
ISSN 2229-5518

In addition to that, the lake's ecosystem has been modified due to lack of water flow into the lake, whether from the Nile or water through Allaqi and Annanah channel which forked from Damietta branch, also less wastewater into the lake, especially after the establishment of Al-Salam Canal which led to the compilation of some of the waste water, which was received by the lake or due to silting Canalize, private Alkaboty in Port Said or two openings of Sheikh and EL Alama on the north coast in Damietta, which led to a lack of salinity of the lake, this helped to growth of weed and the water plants.

Interestingly, the 1984-2015 change detection maps, Figure (11), show also increase in urbanization. Most urban growth is occurring through the building of new communities on the previous desert land and urban sprawl in previously agricultural areas. The total area of the communities civilized newly created in the desert equal 37405ha and are stationed in the east of the capital, Cairo, such as the Tenth of Ramadan, Badr, Al Shrouk, Al Obour, New Al Rehab, El Salam, and Al Salheyah cities as shown in Figure (15). On other hand, the total areas which change from agricultural land to urban in this period equal to 27317 ha in the west and North West of the study area.

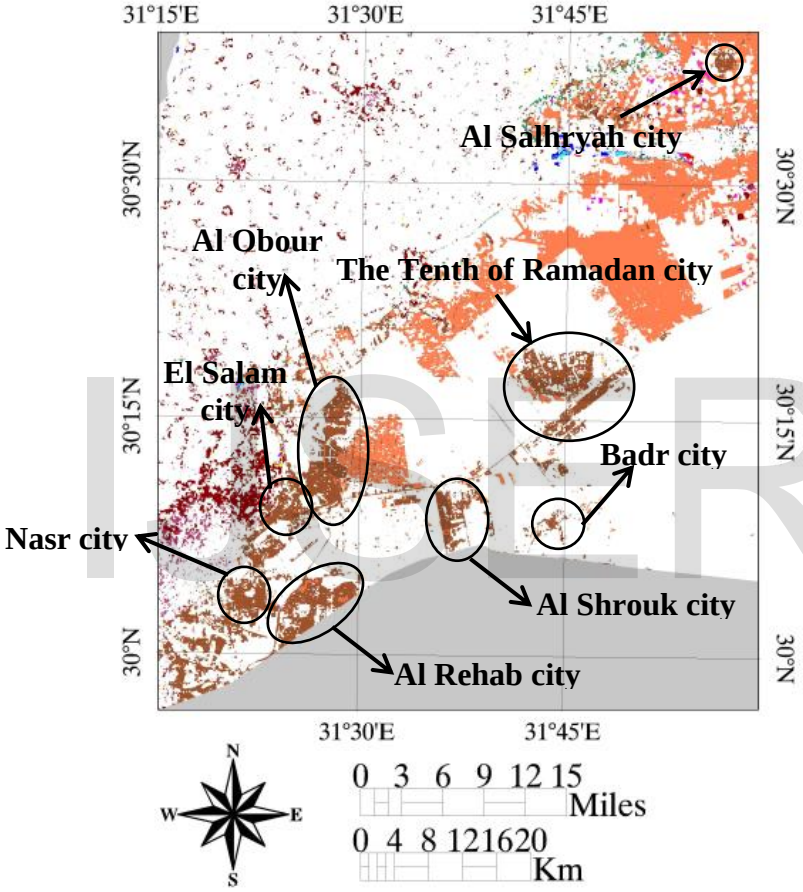

Fig. (15): New cities that appear in period between 1984-2015.

4 Conclusion

In this study, the remote sensing data in terms of multi-spectral and multi-temporal imageries were used to delineate and quantify land-use changes in the eastern Nile Delta Region, Egypt. Landsat images representing 31 year period, acquired in 1984, 1990, 1998, 2006, and 2015. This data was Geo-referenced by a digital topographic map, and corrected geometrically, and radiometrically. Six land-use classes (urban, agriculture, fallow, desert, water and marshland) representing the dominant land cover types in the study area. Land use changes were detected through using a hybrid classification approach. First, the unsupervised interactive self-organizing data analysis (ISODATA) is applied to help in determination of training samples. Then four different supervised classification algorithms, Maximum likelihood, Minimum distance, Mahalanobis Distance and Spectral Angle Mapper, were implemented to produce five land use maps. The maximum likelihood method showed higher classification accuracies in comparison with other methods.

The results show that agricultural and fallow lands classes increases by 8.6 % from year 1984 to 2015 where the average annual rate of land reclamation during 1984-1990 was 7167 ha/year and during 2006-2015 was 2383 ha/year. Between 1984 and 2015 there are four important zones of change appears extensive agricultural development. Due to agriculture developments in this

zone some environmental problems appear, which include groundwater seepage to the surface, increase in soil salinity, lack of rational water resources management in Nile Delta and agricultural pollutants contaminating the groundwater.

Also, during the study period the urbanization increase by 4.8 % (74293 ha), most urban growth is occurring through the building of new communities on the previous desert land and urban sprawl in previously agricultural areas. On the other hand, the desert, surface water and marshland areas have decreased due to increase of urban and agricultural area.

Finally, the use of remote sensing data provides a cost-effective tool to obtain valuable information for better grasp and monitoring land development patterns and processes. Also, change detection information may help to explain local changes observed in water level and groundwater quality.

5 References

[1] P. Dbbeler and N. E. Nannenga-Bremekamp, *New Text Document*, vol. 48, no. 2. 2001, pp. 235–238.

[2] H. R. El-Ramady, S. M. El-Marsafawy, and L. N. Lewis, "Sustainable agriculture and climate changes in Egypt," in *Sustainable agriculture reviews*, Springer, 2013, pp. 41–95.

[3] A. Shalaby and R. Tateishi, "Remote sensing and GIS for mapping and monitoring land cover and land-use changes in the Northwestern coastal zone of Egypt," *Appl. Geogr.*, vol. 27, no. 1, pp. 28–41, 2007.

[4] R. S. DeFries and J. R. G. Townshend, "Global land cover: comparison of ground-based data sets to classifications with AVHRR data," *Environ. Remote Sens. from Reg. to Glob. scales*, vol. 84, 1994.

[5] A. M. Faid and A. M. Abdulaziz, "Monitoring land-use change-associated land development using multitemporal Landsat data and geoinformatics in Kom Ombo area, South Egypt," *Int. J. Remote Sens.*, vol. 33, no. 22, pp. 7024–7046, 2012.

[6] E. Matthews, "Global vegetation and land use: New high-resolution data bases for climate studies," *J. Clim. Appl. Meteorol.*, vol. 22, no. 3, pp. 474–487, 1983.

[7] D. P. Roy, P. E. Lewis, and C. O. Justice, "Burned area mapping using multi-temporal moderate spatial resolution data A bi-directional reflectance model-based expectation approach," *Remote Sens. Environ.*, vol. 83, no. 1, pp. 263–286, 2002.

[8] J. E. Vogelmann, D. Helder, R. Morfitt, M. J. Choate, J. W. Merchant, and H. Bulley, "Effects of Landsat 5 Thematic Mapper and Landsat 7 Enhanced Thematic Mapper Plus radiometric and geometric calibrations and corrections on landscape characterization," *Remote Sens. Environ.*, vol. 78, no. 1, pp. 55–70, 2001.

[9] F. Yuan, K. E. Sawaya, B. C. Loeffelholz, and M. E. Bauer, "Land cover classification and change analysis of the Twin Cities (Minnesota) Metropolitan Area by multitemporal Landsat remote sensing," *Remote Sens. Environ.*, vol. 98, no. 2, pp. 317–328, 2005.

[10] A. M. Abdulaziz, J. M. Hurtado J, and R. Al-Douri, "Application of multitemporal Landsat data to monitor land cover changes in the Eastern Nile Delta region, Egypt," *Int. J. Remote Sens.*, vol. 30, no. 11, pp. 2977–2996, 2009.

[11] J. C.-W. Chan, K.-P. Chan, and A. G.-O. Yeh, "Detecting the nature of change in an urban environment: A comparison of machine learning algorithms," *Photogramm. Eng. Remote Sensing*, vol. 67, no. 2, pp. 213–226, 2001.

[12] D. M. Muchoney and B. N. Haack, "Change detection for monitoring forest defoliation," *Photogramm. Eng. Remote Sensing*, vol. 60, no. 10, pp. 1243–1251, 1994.

[13] A. Singh, "Review article digital change detection techniques using remotely-sensed data," *Int. J. Remote Sens.*, vol. 10, no. 6, pp. 989–1003, 1989.

[14] R. K. Kaufmann and K. C. Seto, "Change detection, accuracy, and bias in a sequential analysis of Landsat imagery in the Pearl River Delta, China: econometric techniques," *Agric. Ecosyst. Environ.*, vol. 85, no. 1, pp. 95–105, 2001.

[15] J. Helmschrot and W.-A. Flügel, "Land use characterisation and change detection analysis for hydrological model parameterisation of large scale afforested areas using remote sensing," *Phys. Chem. Earth, Parts A/B/C*, vol. 27, no. 9, pp. 711–718, 2002.

[16] E. F. Lambin and D. Ehrlich, "Land-cover changes in sub-Saharan Africa (1982--1991): Application

of a change index based on remotely sensed surface temperature and vegetation indices at a continental scale," *Remote Sens. Environ.*, vol. 61, no. 2, pp. 181–200, 1997.
[17] A. R. Palmer and A. F. van Rooyen, "Detecting vegetation change in the southern Kalahari using Landsat TM data," *J. Arid Environ.*, vol. 39, no. 2, pp. 143–153, 1998.
[18] F. Rembold, S. Carnicelli, M. Nori, and G. A. Ferrari, "Use of aerial photographs, Landsat TM imagery and multidisciplinary field survey for land-cover change analysis in the lakes region (Ethiopia)," *Int. J. Appl. Earth Obs. Geoinf.*, vol. 2, no. 3, pp. 181–189, 2000.
[19] A. Etter and others, "Multitemporal analysis (1940--1996) of land cover changes in the southwestern Bogota highplain (Colombia)," *Landsc. Urban Plan.*, vol. 59, no. 3, pp. 147–158, 2002.
[20] M. Malmir, M. M. K. Zarkesh, S. M. Monavari, S. A. Jozi, and E. Sharifi, "Urban development change detection based on Multi-Temporal Satellite Images as a fast tracking approach a case study of Ahwaz County, southwestern Iran," *Environ. Monit. Assess.*, vol. 187, no. 3, pp. 1–10, 2015.
[21] H. Tran, T. Tran, and M. Kervyn, "Dynamics of land cover/land use changes in the Mekong delta, 1973--2011: A remote sensing analysis of the Tran Van Thoi District, Ca Mau Province, Vietnam," *Remote Sens.*, vol. 7, no. 3, pp. 2899–2925, 2015.
[22] Z. Hassan *et al.*, "Dynamics of land use and land cover change (LULCC) using geospatial techniques: a case study of Islamabad Pakistan," *Springerplus*, vol. 5, no. 1, pp. 1–11, 2016.
[23] S. A. Sadek, "Use of landsat imagery for monitoring agricultural expansion of East and West Nile Delta, Egypt," *Egypt. J. Soil Sci.*, 1993.
[24] M. P. Lenney, C. E. Woodcock, J. B. Collins, and H. Hamdi, "The status of agricultural lands in Egypt: the use of multitemporal NDVI features derived from Landsat TM," *Remote Sens. Environ.*, vol. 56, no. 1, pp. 8–20, 1996.
[25] E. A. El Gammal, S. M. Salem, and A. E. A. El Gammal, "Change detection studies on the worlds biggest artificial lake (Lake Nasser, Egypt)," *Egypt. J. Remote Sens. Sp. Sci.*, vol. 13, no. 2, pp. 89–99, 2010.
[26] A. Shalaby and F. S. Moghanm, "Assessment of urban sprawl on agricultural soil of northern Nile Delta of Egypt using RS and GIS," *Chinese Geogr. Sci.*, vol. 25, no. 3, pp. 274–282, 2015.
[27] E. S. Ammeish, B. M. Mabrouk, and W. S. Morsy, "RS and GIS Based Approach for Detecting Landuse Changes and its Impact on the Groundwater Aquifer," *Life Sci. J.*, vol. 13, no. 4, 2016.
[28] H. H. Elewa, R. E. Shohaib, A. A. Qaddah, and A. M. Nousir, "Determining groundwater protection zones for the Quaternary aquifer of northeastern Nile Delta using GIS-based vulnerability mapping," *Environ. earth Sci.*, vol. 68, no. 2, pp. 313–331, 2013.
[29] S. M. Zaid, "Geo-environmental study of Eastern Nile Delta, Egypt," PhD thesis. Faculty of Science, Zagazig University, Egypt, p 339, 2006.
[30] A. Masria, K. Nadaoka, A. Negm, and M. Iskander, "Detection of Shoreline and Land Cover Changes around Rosetta Promontory, Egypt, Based on Remote Sensing Analysis," *Land*, vol. 4, no. 1, pp. 216–230, 2015.
[31] D. A. Stow, "Reducing mis-registration effects for pixel-level analysis of land-cover change," *Int. J. Remote Sens.*, vol. 20, no. 12, pp. 2477–2483, 1999.
[32] M. E. Hereher, "Mapping coastal erosion at the Nile Delta western promontory using Landsat imagery," *Environ. Earth Sci.*, vol. 64, no. 4, pp. 1117–1125, 2011.
[33] R. S. Lunetta, C. D. Elvidge, and others, *Remote sensing change detection: environmental monitoring methods and applications*. Taylor & Francis Ltd, 1999.
[34] M. Louati, H. Sa"\idi, and F. Zargouni, "Shoreline change assessment using remote sensing and GIS techniques: a case study of the Medjerda delta coast, Tunisia," *Arab. J. Geosci.*, vol. 8, no. 6, pp. 4239–4255, 2015.
[35] M. Elhag, A. Psilovikos, and M. Sakellariou-Makrantonaki, "Land use changes and its impacts on water resources in Nile Delta region using remote sensing techniques," *Environ. Dev. Sustain.*, vol. 15, no. 5, pp. 1189–1204, 2013.
[36] H. M. Reese *et al.*, "Statewide land cover derived from multiseasonal Landsat TM data: a retrospective of the WISCLAND project," *Remote Sens. Environ.*, vol. 82, no. 2, pp. 224–237, 2002.

International Journal of Scientific & Engineering Research, Volume 7, Issue 12, December -2016
ISSN 2229-5518

[37] ENVI, (2014). ENVI version 5.3 user tutorials August edition. ITT Visual Information Solutions, 20REF47DOC.
[38] J. R. Jensen, "Digital change detection," *Introd. Digit. image Process. A Remote Sens. Perspect.*, pp. 467–494, 2004.
[39] M. Chi, R. Feng, and L. Bruzzone, "Classification of hyperspectral remote-sensing data with primal SVM for small-sized training dataset problem," *Adv. Sp. Res.*, vol. 41, no. 11, pp. 1793–1799, 2008.
[40] J. A. Richards and J. A. Richards, *Remote sensing digital image analysis*, vol. 3. Springer, 1999.
[41] H. Vahidi, "Evaluation of the Pixel Based and Object Based Classification Methods For Monitoring Of Agricultural Land Cover Case study: Biddinghuizen-The Netherlands." Geomatics, 2010.
[42] F. A. Kruse *et al.*, "The spectral image processing system (SIPS) interactive visualization and analysis of imaging spectrometer data," *Remote Sens. Environ.*, vol. 44, no. 2, pp. 145–163, 1993.
[43] E. L. Hunter and C. H. Power, "An assessment of two classification methods for mapping Thames Estuary intertidal habitats using CASI data," *Int. J. Remote Sens.*, vol. 23, no. 15, pp. 2989–3008, 2002.
[44] D. Lu, P. Mausel, E. Brondizio, and E. Moran, "Change detection techniques," *Int. J. Remote Sens.*, vol. 25, no. 12, pp. 2365–2401, 2004.
[45] O. Hall and G. J. Hay, "A multiscale object-specific approach to digital change detection," *Int. J. Appl. Earth Obs. Geoinf.*, vol. 4, no. 4, pp. 311–327, 2003.
[46] M. K. Ridd and J. Liu, "A comparison of four algorithms for change detection in an urban environment," *Remote Sens. Environ.*, vol. 63, no. 2, pp. 95–100, 1998.
[47] R. Peiman, "Pre-classification and post-classification change-detection techniques to monitor land-cover and land-use change using multi-temporal Landsat imagery: a case study on Pisa Province in Italy," *Int. J. Remote Sens.*, vol. 32, no. 15, pp. 4365–4381, 2011.
[48] D. Yuan, C. D. Elvidge, and R. S. Lunetta, "Survey of multispectral methods for land cover change analysis," 1998.
[49] P. Coppin, I. Jonckheere, K. Nackaerts, B. Muys, and E. Lambin, "Review ArticleDigital change detection methods in ecosystem monitoring: a review," *Int. J. Remote Sens.*, vol. 25, no. 9, pp. 1565–1596, 2004.
[50] R. G. Congalton and K. Green, *Assessing the accuracy of remotely sensed data: principles and practices*. CRC press, 2008.
[51] R. Congalton and R. A. Mead, "A quantitative method to test for consistency and correctness in photointerpretation," *Photogramm. Eng. Remote Sens.*, vol. 49, no. 1, pp. 69–74, 1983.
[52] O. R. A. El-Kawy, J. K. Rød, H. A. Ismail, and A. S. Suliman, "Land use and land cover change detection in the western Nile delta of Egypt using remote sensing data," *Appl. Geogr.*, vol. 31, no. 2, pp. 483–494, 2011.
[53] A. K. Hegazy, M. A. Medany, H. F. Kabiel, and M. M. Maez, "Spatial and temporal projected distribution of four crop plants in Egypt," in *Natural Resources Forum*, 2008, vol. 32, no. 4, pp. 316–326.